International Journal of Energy Research

INTERNATIONAL JOURNAL OF ENERGY RESEARCH
Int. J. Energy Res. 2016; **40**:1712–1723
Published online 18 May 2016 in Wiley Online Library (wileyonlinelibrary.com). DOI: 10.1002/er.3559

RESEARCH ARTICLE

Transport, thermodynamic, and structural properties of rare earth zirconia-based electrolytes by molecular dynamics simulation

Mohammad Razmkhah[1], Mohammad Taghi Hamed Mosavian[1] and Fatemeh Moosavi[2,*,†]

[1]Department of Chemical Engineering, Ferdowsi University of Mashhad, Mashhad, 9177948944, Iran
[2]Department of Chemistry, Ferdowsi University of Mashhad, Mashhad, 9177948974, Iran

SUMMARY

Rare earth zirconia-based electrolytes were investigated by molecular dynamics simulation in a spanning temperature of 1373 K to 1873 K in order to evaluate whether dopant size plays any role in ionic conductivity of oxygen ions. A new aspect of vibrational analysis was introduced to explain trend of the slope of Arrhenius plots (migration movement barrier, MMB). Vibrational spectra of atomic trajectory of cations and anions were calculated by Fourier transform analysis. The result demonstrates that electrolyte with smaller dopant suggests lower vibration in hopping plate cations (HPCs) and was verified by Zr^{4+} mean square displacement (MSD). Result of MSD indicated that dopant which is heavier (atomic mass) than Zr implies higher movement (or vibration). Thus, dopant vibration is responsible for MMB. A simple well-defined model was applied to investigate activation energy of oxygen ion hopping. It was found that lower vibrating HPC electrolyte deduces lower activation energy. First peak of O–O radial distribution function and 001 density distribution of oxygen ions claimed activation energy of oxygen hopping has direct correlation with oxygen scattering in the lattice structure. Thermal expansion and heat capacity as well were studied as important factors in heating operation. Although, results did not show relation between dopant size and these two thermal factors, it was found a linear relation between van der Waals and kinetic energy, respectively. Copyright © 2016 John Wiley & Sons, Ltd.

KEY WORDS

activation energy; heat capacity; ionic conductivity; molecular dynamics simulation; rare earth; solid oxide fuel cell (SOFC); thermal expansion; vibrational spectra

Correspondence

*Fatemeh Moosavi, Department of Chemistry, Ferdowsi University of Mashhad, Mashhad 9177948974, Iran.
†E-mail: moosavibaigi@um.ac.ir

Received 16 December 2015; Revised 7 April 2016; Accepted 17 April 2016

1. INTRODUCTION

In the recent century, as the industry has been growing, consumption of carbon-containing fuel has extensively increased. This huge rate of burning fuel has resulted from two grand challenges in front of world society. Global warming and reduction of energy sources are the significant challenges. Discovering the problem and public awareness for environmental protection led to enormous research fields concentrating on the alternative renewable-energy technology such as wind turbine, photovoltaic, micro-turbine, fuel cell, etc.

Fuel cell is one of the most promising technologies, which converts gaseous fuels (hydrogen, natural gas, and gasified coal) via an electrochemical process directly into electricity. Research work in the field of fuel cell technology has grown exponentially [1] because of its chief advantages that are high efficiency, flexibility of operation, continuous energy production, and low pollutant emission.

Among different types of fuel cell, solid oxide fuel cell (SOFC) is the most efficient energy generator constructed from a solid oxide electrolyte. Because of high operating temperature, fossil fuels can be reformed within the cell stack, eliminating the need for an expensive and external reformer. Additionally, utilizing a variety of hydrocarbon fuels from renewable fuel such as biomass (fuel flexibility) [1] and possibility of exploiting a wide range of applications, ranging from portable power units to stationary power cogeneration systems [2], are other great advantages of SOFC in comparison with other types of fuel cells.

Although operating at a high temperature has some advantages, it limits commercializing SOFC. Operating at high-temperature demands applying expensive materials for fuel cell interconnectors, long start-up time, and large

energy input to heat the cell up to the operating temperature [3]; thereby, the major concern is to reduce the temperature. As shown previously, it is impossible to solve the problem without deep understanding about electrolyte [4]. Actually, at the top of 'electrolyte analysis', investigating the behavior of 'oxygen ion' is the foremost criteria in SOFC electrolyte. There has been a debate what the principal barrier against oxygen ion hopping is. As the current research demonstrates, there may be a relation between the oxygen ion hopping and vibration of neighbor cations. In addition, the activation energy was modeled to rationalize barrier against oxygen ion hopping. We are also enthusiastic over knowing whether any relation is observed between ionic size of dopant and oxygen movements. Accordingly, some rare-earth dopants were selected to study this relation.

High operating temperature also demands to inspect thermal expansion and heat capacity. In fact, thermal expansion of cathode, anode, and electrolyte must be matched together. This important property limits selection of materials. Besides, heat capacity of electrolyte provides some information about the electrolyte heat response. In other words, because of showing how much energy one electrolyte requires changing its temperature, heat capacity comes into effect. Overall, these thermodynamic properties are important in startup operation. The current research attempts mainly to answer this question if there is any relation between these thermodynamic properties and size of dopant.

The main requirements for an electrolyte are high ionic conductivity, low electronic conductivity, stability in both oxidizing and reducing environments, good mechanical properties, and long-term resistance under operating condition [3]. According to the wide application, zirconia-based electrolytes have attracted more attention than other oxygen-ion conductors [5]. Zirconia-based electrolytes are generally electronic insulator materials because a closed shell electronic structure of each ion prevents movement of electrons. At high enough temperature, the ions translate through the solid, so-called ionic conductivity. Such ion conductor materials at temperatures below the melting point exhibit a liquid-like motion while they are in solid phase. This unusual behavior has attracted great attention to this group of materials [6].

From empirical point of view, various approaches have been proposed to enhance the ionic conductivity of zirconia-based oxide electrolytes with composition variation. Experimental studies suggest that oxygen ion conductivity in doped zirconia depends on ion size of the dopant cation as well as its concentration. In the literature, some people have recognized that size difference has influence on the energy of association [7,8]. Furthermore, Arachi *et al*. [9] have reported conductivity of the systems containing ZrO_2–Ln_2O_3 (Ln = lanthanides) decreases with ion radius of dopant. Really, effect of dopant size has been studied experimentally, but in this study, there was an attempt to investigate the effect of rare-earth dopant size, which is not considered before theoretically, and introduce some new analysis methods by MD simulation in order to explore ionic conductivity behavior of such electrolytes.

Studying zirconia-based electrolyte can be carried out by computer simulation that is considered as a supplement to experiment. Simulation acts as a bridge between microscopic and macroscopic world. Computer simulation by a theoretical model containing the interactions between atoms, molecules, and ions as an input is able to predict the properties of a system.

Conducting molecular dynamics (MD) simulation before experimental studies provides deep insight into the effective variables of the system. Furthermore, because experimental examination is based on trial and error and solid oxide electrolyte materials are expensive, it is more appropriate to use MD technique to predict material characteristics.

The early molecular dynamic studies in the field of zirconia based solid oxide electrolyte focused on oxygen diffusion in YSZ electrolyte [10–14]. In such studies, effect of temperature on oxygen diffusion was introduced as typical analysis [15–20]. One of the first MD simulations studies on the subject of the effect of rare-earth dopant (Yb) on ionic conductivity of zirconia based electrolyte was carried out by Pramananda *et al*. [21]. In fact, this study introduced the rare-earth dopant as a promising material to improve ionic conductivity of oxygen ion. The other studies in this field concentrated on the effect of combination of two different dopants [22–24]. Actually, brilliant effect of rare-earth material on oxygen diffusion motivated following studies to apply a combination of dopant in such electrolytes. Accordingly, in the present study, we focus on these materials and attempt to investigate their ionic conductivity behavior. With this regard, in the current work, detailed investigation on the effect of rare-earth dopant on zirconia-based electrolyte was carried out using MD with the following main goals:

- Presenting and comparing rare-earth electrolyte materials
- Studying the effect of temperature on ionic conductivity of target electrolytes
- Investigating ionic conductivity and its relation with dopant size
- Analyzing the conductivity behavior of electrolytes with respect to their structure
- Introducing a new aspect of applying vibrational spectra
- Modeling activation energy in order to analyze solid oxide electrolyte
- Calculating two important thermodynamic properties, thermal expansion and heat capacity

2. SIMULATION METHOD

Molecular dynamics simulations were performed on a cubic box with edges of 16 Å containing 324 ions of zirconia developed from crystallographic unit cells [25]. Yb, Er, Gd, Nd, Pr, and La ions were doped on zirconia to construct the doped solid oxide electrolyte. In fact, maximum ionic

conductivity occurs about 8–9 mol% of dopant B_2O_3 [5]. As a result, this pilot study constructed all electrolytes at 8 mol% of rare-earth dopant. In addition, results of simulation were compared with the reported experiments [26–30]. Ewald's summation (with precision of 1×10^{-5}) [31] represents long-range electrostatic interactions with full formal ion charges and Born–Mayer–Buckingham potential [32] illustrate short-range interactions:

$$\varphi(r_{ij}) = A_{ij}\exp\left(-\frac{r_{ij}}{\rho_{ij}}\right) - \frac{C_{ij}}{r_{ij}^6} \tag{1}$$

where A_{ij}, C_{ij}, and ρ_{ij} are the potential coefficients and r_{ij} demonstrates the distance between i and j ions. Table I lists short range potential parameters [33]. Cation–anion interactions followed Born–Mayer–Buckingham potential [33] in addition to the long-range electrostatic interactions. Cation–cation interactions were considered to be only Columbic. Simulations at all temperatures were performed in two stages. First, isobaric–isothermal (NPT) ensemble with crystallographic structure as initial configuration was applied. NPT simulations were carried out to control the cell volume vibration with temperature. Berendsen thermostat and barostat [34] controlled temperature and pressure every 0.1 ps and 1 ps, respectively. Second, the final structure of the first stage was used as initial configuration for canonical ensemble (NVT). This stage was carried out to compute mean square displacement (MSD) by applying the same thermostat at each temperature. All simulations were continued up to 10 ns with a time step 1 fs. Verlet algorithm [35] was applied for MD simulation integration method. The cut-off distance was 8 Å for both series of simulations (NPT and NVT), all carried out by DL_POLY 2.17 simulation package [36,37].

The diffusion coefficient, D, was calculated from MSD via Einstein's equation [38]:

$$\frac{1}{N}\sum_{i=1}^{N}[r_i(t) - r_i(0)]^2 = 6Dt + B \tag{2}$$

where r_i is atomic position, t represents time, N corresponds to the total number of the atoms, and B is a constant. MSD plots versus time support the diffusion coefficient values that can be used in order to evaluate ionic conductivity, σ, using Nernst–Einstein relation [38]:

$$\sigma = \frac{nq^2D}{kH_RT} \tag{3}$$

that n represents concentration of mobile ions, q is ionic charge, k is Boltzmann constant, T is temperature, and H_R is Haven ratio equal to 0.65 [39].

Arrhenius equation presents the variation of ionic conductivity with temperature [26]:

$$\sigma = \sigma_0\exp\left(-\frac{E_a}{kT}\right) \tag{4}$$

where E_a is the activation energy of migration, means migration movement barrier (MMB) of ions, and σ_0 is pre-exponential factor.

Fourier transform of trajectory can be obtained from [40]:

$$R(\omega) = \int r_i(t)e^{-J\,\omega\,\pi t}dt \tag{5}$$

where ω is frequency and J is equal to $\sqrt{-1}$.

Analyzing atomic correlation is performed by radial distribution function (RDF):

$$g_{i,j}(r) = \frac{V}{N_j}\frac{N_j(r)}{4\pi r^2\Delta r} \tag{6}$$

where V is cell volume, N_j is total number of j atoms, and $N_j(r)$ is the number of j atoms in a spherical shell of Δr around i atoms.

Isobaric expansion coefficient [41] is defined as:

$$\alpha = \frac{1}{V}\left(\frac{\partial V}{\partial T}\right)_p = \left(\frac{\partial \ln V}{\partial T}\right)_p. \tag{7}$$

This property can be readily obtained from temperature dependence of volume by conducting constant pressure simulations at several temperatures.

Heat capacity at constant volume [42] can be calculated from:

$$C_v = \frac{\langle E^2\rangle - \langle E\rangle^2}{NkT^2} \tag{8}$$

where E is total energy and bracket indicates an average value.

Table I. Potential parameters [33].

Interaction	A_{ij} (eV)	ρ_{ij} (Å)	C_{ij} (eV Å^6)
M–M	0	1	0
Zr–O	1453.80	0.3500	0
O–O	22 764.30	0.149	27.88
Yb–O	1309.60	0.3462	0
Er–O	1739.91	0.3389	17.55
Gd–O	1336.80	0.3551	0
Nd–O	1379.90	0.3601	0
Pr–O	2025.54	0.3427	13.85
La–O	1439.70	0.3651	0
Y–O	1345.10	0.3491	0

*M = Y, Yb, Er, Gd, Nd, Pr, La, and Zr.

Int. J. Energy Res. 2016; **40**:1712–1723 © 2016 John Wiley & Sons, Ltd.
DOI: 10.1002/er

3. RESULTS AND DISCUSSION

3.1. Transport property

One of the most considerable parameters, which plays a critical role in selecting an electrolyte for SOFC application, is ionic conductivity. Dopant ionic size and temperature are two factors that imply great influence on ionic conductivity of electrolyte. In order to investigate these factors, a set of rare-earth zirconia-based electrolytes under spanning range of operating temperature (1373–1873 K) was simulated by MD. Aimed systems are Ytterbium stabilized zirconia (YbSZ), Erbium stabilized zirconia (ErSZ), Gadolinium stabilized zirconia (GdSZ), Neodymium stabilized zirconia (NdSZ), Praseodymium stabilized zirconia (PrSZ), and Lanthanium stabilized zirconia (LaSZ). Ionic radius of each dopant was reported in Table II.

Before studying the effect of ionic size on ionic conductivity, the validity of simulation results was examined that is a very necessary part of investigation. Comparing the results of simulation with experimental data verified simulation results, see Figure 1. The results came to appreciable agreement with experimental data claiming on the acceptability of simulation procedure. MD simulation of LaSZ over-predicted the ionic conductivity compared with experimental data that can be explained by grain boundary. In this study, the grain boundary effect was not included in structural configuration and bulk ionic conductivity was the main target.

Table II. Ionic radius of rare earth ion [43].

Ion	Ionic radius (pm)
Yb^{3+}	98.5
Er^{3+}	100.4
Gd^{3+}	105.3
Nd^{3+}	110.9
Pr^{3+}	112.6
La^{3+}	116.0

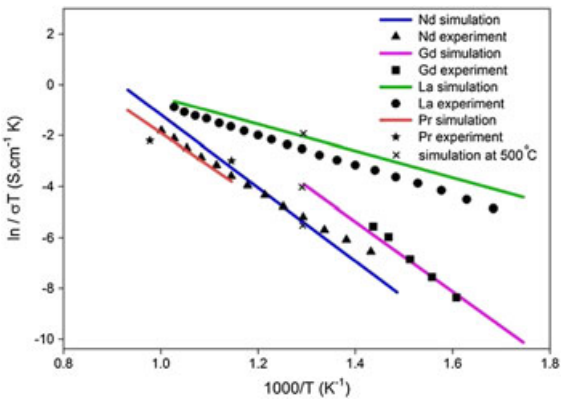

Figure 1. Arrhenius plots of ionic conductivity in comparison with experimental data for some studied electrolyte [26–30].

Arrhenius plot of zirconia-based electrolyte always implies a linear trend from a low-temperature region to high operating temperature. In addition, simulation at elevated temperature (1373–1873 K, 1100–1600 °C) suggests lower simulation costs. Therefore, it is reasonable to carry out simulation at higher temperature and then extend it to the low temperature region. However, we conduct a simulation at the low temperature region (773 K, 500 °C) for LaSZ, NdSZ, and GdSZ as typical samples to verify this claim; see Figure 1.

As explained before, size of dopant and operating temperature affect ionic conductivity of an electrolyte. There is an attempt to show these two effective factors with a plot as can be seen in Figure 2. According to Figure 2, temperature dependence of ionic conductivity showed an Arrhenius behavior in accordance with previous studies (see also Figure 1) [26–30]. Ionic conductivity trend toward dopant size exposed different characteristics from low operating temperature to high operating temperature. Surprisingly, it was observed at low and intermediate temperature region ionic conductivity values of LaSZ and YbSZ are higher than commercial electrolyte, YSZ. The slope of Arrhenius plot is responsible for such behavior. Therefore, investigating the effective parameter of this property may help to find appropriate electrolyte in the future.

According to Badwal's study [5], ionic size of dopant plays a significant role in ionic conductivity of electrolyte, but the trend at low temperatures is not the same at high ones, see Figure 2. Therefore, the current study investigates the slope of Arrhenius plot because it can be characteristic for the ionic conductivity and does not rest on temperature. Actually, slope of Arrhenius plot shows the dynamic behavior of particle in the electrolyte at the low temperature region. Figure 3 shows the MMB (slope of Arrhenius plot) of the electrolytes as a function of ionic size of dopant. It can clearly be seen that there has been a noticeable increase in slope of ionic conductivity until 110.9 Å followed by a marked decrease after this point. Now, the question is what occurs and why we observe such behavior. Answering to these questions demands to recognize structural behavior of the electrolytes.

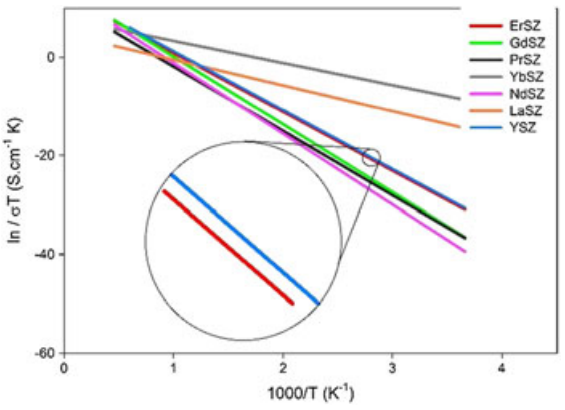

Figure 2. Arrhenius plots of ionic conductivity for simulated electrolytes.

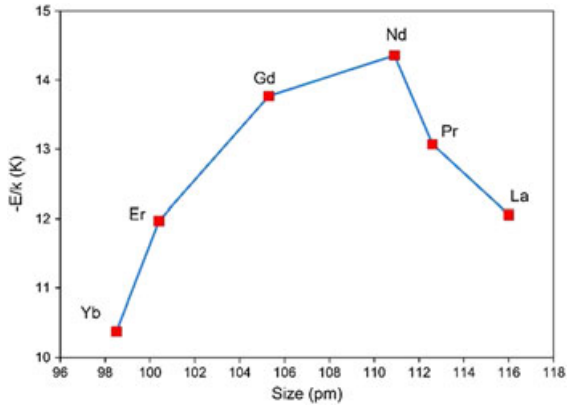

Figure 3. Slope of Arrhenius plot for simulated electrolytes.

3.2. Structural analysis

3.2.1. Atomic vibration

In order to explain the new method of atomic vibration analysis, it is vital to classify oxygen ion into dynamic oxygen ion (DOI) and static oxygen ion (SOI). Actually, those oxygen ions hopping to vacancy are called DOI and the other oxygen ions, which only vibrate in their locations, are SOI. We believe dynamic behavior of oxygen depends on vibration of cation and anion. Accordingly, in current research, a traditional method was used that is applicable in analysis of mechanical vibrations. The idea of this analysis stems from considering cations as vibrating units and using the vibration analysis to understand the behavior of lattice structure. DOI and free space between the cations were under consideration to demonstrate the effect of cation vibration on oxygen ionic conductivity. Indeed, DOI should hop through the cation plate to result in ionic conductivity through the electrolyte [23]. Subsequently, accessible free space between cations plays an inevitable role in oxygen hopping process. Logically, we believe vibrating cations fill the free space in the lattice; the least cation vibration one electrolyte has the most ionic conductivity it may experience.

Analysis with this method was divided into two steps: (i) evaluating vibrational spectra and (ii) finding the behavior of the cation plate. Vibrational spectra can be calculated from Fourier transform of atomic trajectory [44]. Using these spectra helps to compare the vibration of different cations in target electrolytes. In this study, a DOI was selected randomly and vibrational spectra of cations surrounding in cubic shape were considered. A DOI should cross through the face of surrounded cube. Accordingly, the cation lattice encompassing DOI from the perspective of hopping plate was divided into: (i) cationic plate through which DOI hops naming hopping plate cations (HPC) and (ii) other cations which DOI does not cross through their plate and are named non-hopping plate cations (NHPC), both illustrated in Figure 4. Vibrational spectra of HPC and NHPC were plotted in Figure 5. As can be clearly

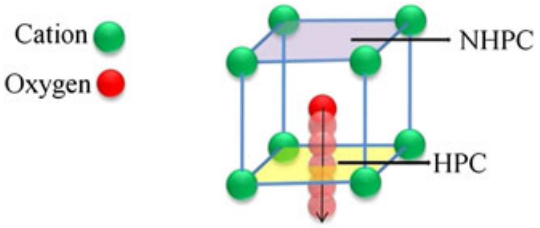

Figure 4. Scheme of HPC and NHPC.

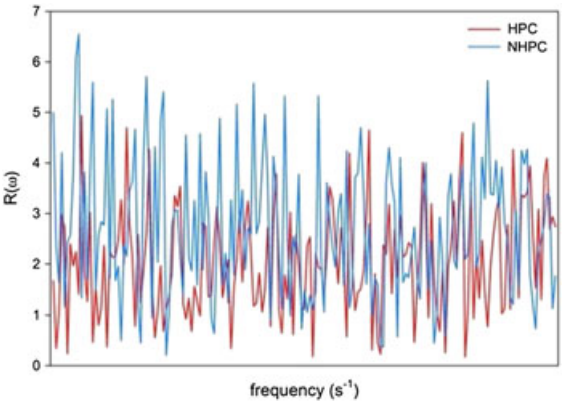

Figure 5. Vibrational spectra of HPC and NHPC at 1373 K.

seen, vibration of HPC was higher than NHPC; thus, cation vibration is a barrier against oxygen hopping. In other words, such vibration restricts the accessible oxygen crossing area.

A comparison between HPC of YbSZ and NdSZ electrolytes with the highest and lowest MMB, as a typical sample, is shown in Figure 6. This figure clarifies the effect of cation vibration on oxygen MMB. According to vibration amplitude, vibration of cations in YbSZ electrolyte is lower than NdSZ. Consequently, it is reasonable to conclude a low oxygen MMB of a system sheds light on free space or accessible surface area.

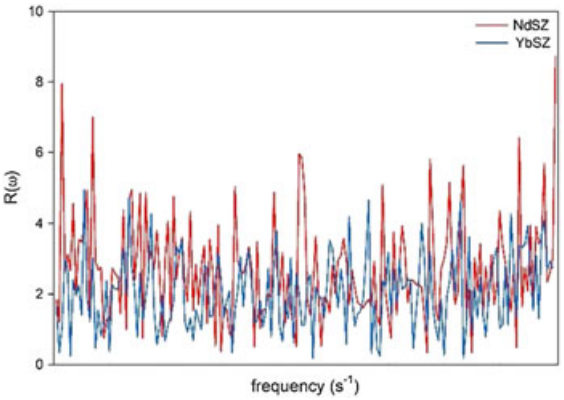

Figure 6. HPC of NdSZ versus YbSZ at 1373 K.

Int. J. Energy Res. 2016; **40**:1712–1723 © 2016 John Wiley & Sons, Ltd.
DOI: 10.1002/er

Unlike to cations, we expect the electrolyte with lower oxygen MMB exposes higher oxygen ion vibration because vibration of oxygen conducts hopping process. Figure 7 shows the vibration of oxygen ion of the lowest and the highest MMB, i.e. YbSZ and NdSZ. As figure demonstrates, the electrolyte with the lowest oxygen MMB has the highest oxygen vibration. To sum up, the greater oxygen vibration and the lower HPC vibration one electrolyte has, the higher ionic conductivity it may experience.

Studying the vibration of cation assists to define a property entitled 'activation energy'. Vibration of cations causes to increase activation energy of the hopping oxygen from its site to the nearest vacancy site. Consequently, investigating activation energy may provide valuable information about the MMB of oxygen in the systems.

3.2.2. Modeling the activation energy

There was an attempt to interpret MMB trend of electrolyte. Thus, a simple model was provided to clear up unknown part of oxygen MMB trend. This model only considers one cube with four cations on corner points and one DOI on the center of the cube. We assume the cations are fixed in their position. In addition, repulsive and attractive forces are exerted on DOI to calculate hopping activation energy. Total force acting on each cation must be balanced to stabilize them in their position. Thus, some negative charges, which are because of neighboring oxygen, should be considered on each cationic site to neutralize the modeled cube structure. The charge of each cation was noted by a and the central oxygen charge which should be distributed over the cations was noted by b; the amount of negative charge of adjacent oxygen, given as c, is calculated by $c = a - b$. The distributed central oxygen charge, b, is calculated as below:

Each Zr^{4+} requires four negative charges while dopant^{3+} needs three negative charges to be stable; as a result, $\frac{4}{3+4}$ of central oxygen charge is considered for each Zr^{4+} and $\frac{3}{3+4}$ for each dopant. Therefore, by considering formal oxygen charge, the portion of Zr^{4+} cation is $\frac{4}{3+4} \times 2 = 1.14$ and $\frac{3}{3+4} \times 2 = 0.86$ for dopant^{3+}. Besides, as Figure 8a shows, the oxygen is surrounded by four Zr^{4+} and four dopant^{3+}; it can be concluded that the portion for each Zr^{4+} and each dopant^{3+} is $\frac{1.14}{4} = 0.29$ and $\frac{0.86}{4} = 0.21$, respectively. Accordingly, $4 - 0.29 = 3.71$ ($c = a - b$) and $3 - 0.21 = 2.79$ ($c = a - b$) negative charges are located on each Zr^{4+} site and each dopant^{3+} site, respectively. At the beginning, oxygen ion is located in the relaxation point of the lattice and then moves through the plate. It is also assumed that oxygen ion crosses through the minimum point of energy of any plate (see Figure 8a); as a result, cube faces, which surround anion, play the main role in anion transferring. At present, the question is which cube face is the most favored for oxygen crossing.

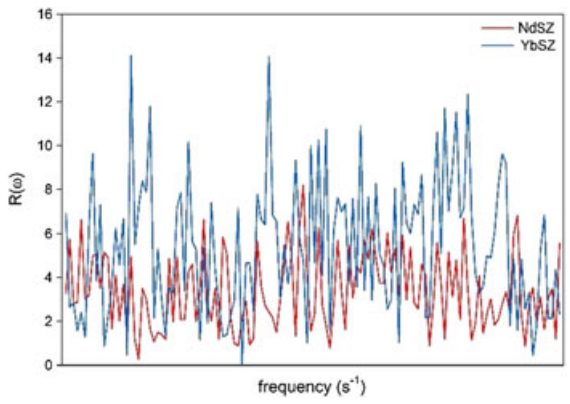

Figure 7. Oxygen vibrational spectra of NdSZ versus YbSZ at 1373 K.

Each cube has six faces, but according to the configuration applied in this study, there are only two different plates, see Figure 8b. Thus, there are two scenarios for oxygen crossing through the plate (plate 1 and 2 in Figure 8 b): a) moving from its relaxation point to the minimum energy point of the plate 1, b) or plate 2. The model showed scenario 1 is more probable because its energy is lower than scenario 2; accordingly, plate 1 was selected to compare activation energy of oxygen hop in each electrolyte. Activation energy of oxygen hopping was calculated from the difference between oxygen relaxation energy in each system from its minimum energy of plate 1:

$$\Delta E_i = E_{relaxation_i} - E_{plate1_i} \tag{9}$$

where $E_{\text{relaxation}}$ is the energy at relaxation point, E_{plate1} is the minimum energy calculated from scenario 1, and i shows aimed electrolyte.

Modeled activation energy of electrolytes was reported in Figure 9. As one can see, the activation energy follows the same trend as MMB plot, Figure 3. Now, it is clear, to some extent, that DOI in NdSZ system needs more energy to cross through its plate. It also agrees with the result of vibrating cations. Consequently, it may be reasonable that the higher MMB one electrolyte has, the higher activation energy it experiences.

3.2.3. Oxygen ion distribution and structure ordering

A solid-state structure like zirconia prefers to be in an ordered form. Dopant with a lower ionic charge creates defects in the zirconia structure. Such defects attract oxygen ions and obligate them to hop. However, oxygen ions do not move in an electrolyte without any limitation. They just move in an identified direction and stand in particular sites. Now the main challenge is any relation between the oxygen MMB and structure ordering. Figure 10 shows distribution of cation for YbSZ, NdSZ, and LaSZ along 001 direction. The figure shows YbSZ has a tighter distribution than NdSZ and LaSZ. As mentioned already, the electrolyte with higher MMB has higher cationic vibration; thus, higher disordering is expected. This high disordering in such systems may cause high-scattered cation in the system.

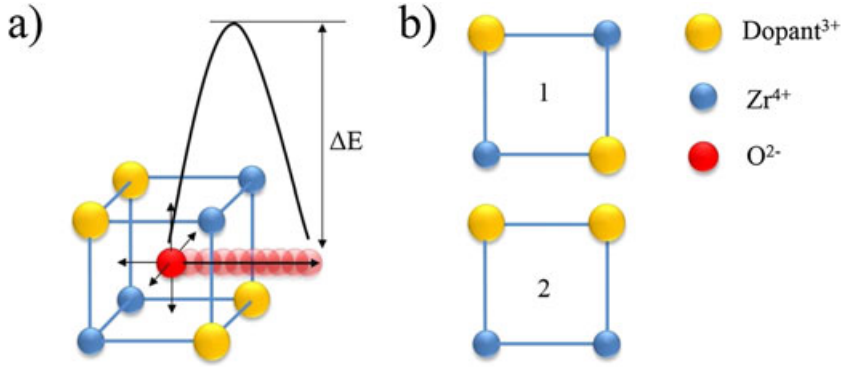

Figure 8. a) Scheme of activation energy b) two probable plates for oxygen hopping.

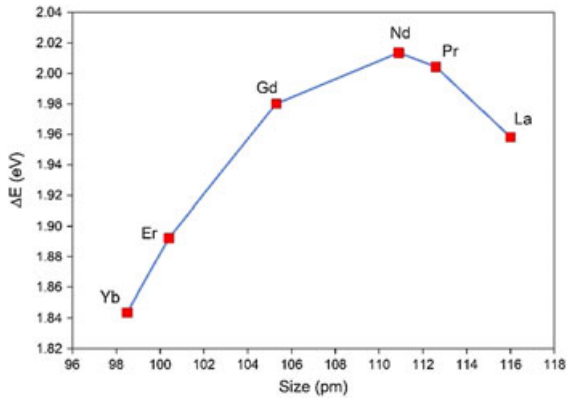

Figure 9. Modeled activation energy for studied electrolytes.

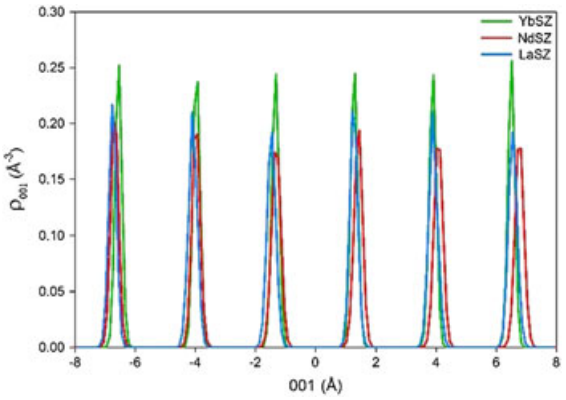

Figure 10. Atomic density of cations in 001 direction at 1373 K.

In addition, oxygen is confined between the corner cations in the lattice; hence, disordering of cations leads to disordering of the oxygen in the electrolyte as shown in Figure 11.

3.2.4. RDF analysis

Another structure analysis, RDF, was used to investigate how particles distribute around a specific particle. As discussed above, oxygen ions of the highest oxygen MMB system experience the highest scattering in lattice space. Low height of peak with wide distribution in RDF plot points to the high-scattered particles. Pair correlation function of O–O supports the trend of oxygen distribution in each electrolyte. As shown in Figures 12a and b, height of first peak in each electrolyte results a trend in contrast to oxygen MMB plot (Figure 3), i.e. high MMB system enjoys a high scattered oxygen. In addition, this result is in agreement with the distribution in 001 direction, Figures 10 and 11.

3.2.5. MSD of cations

Disordering of electrolytes was investigated by 001 density distribution and RDF of O–O pair. MSD analysis is a powerful tool to investigate the movement of ions. From the other side of view, MSD plot may give some information that sheds light on atomic vibration. It is

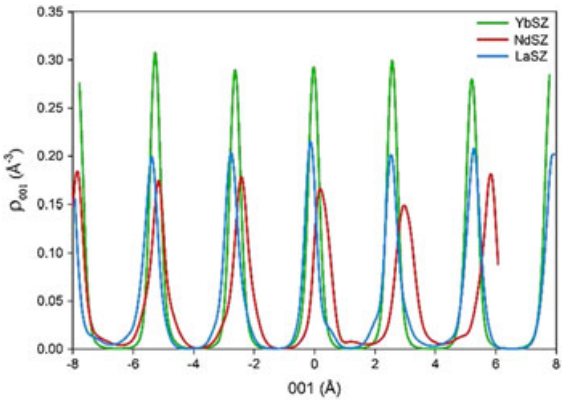

Figure 11. Atomic density of oxygen ions in 001 direction at 1373 K.

proposed that the higher vibration one system has, the higher MSD it may experience. Therefore, MSD plot of cations (especially Zr^{4+}) may also confirm vibration discussed above. Figure 13 compares MSD of Zr^{4+} of target electrolytes. As the figure shows, MSD of NdSZ is greater than YbSZ; as a result, the vibration or movement of NdSZ is also high.

Int. J. Energy Res. 2016; **40**:1712–1723 © 2016 John Wiley & Sons, Ltd.
DOI: 10.1002/er

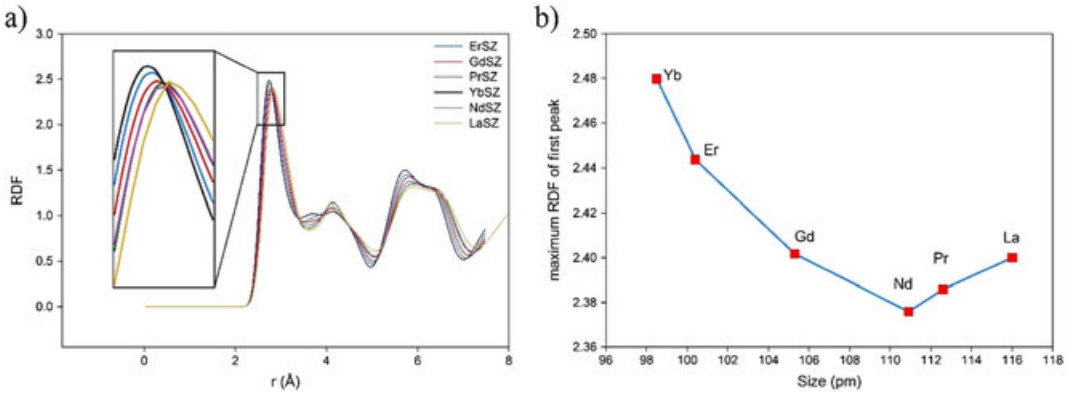

Figure 12. a) Radial distribution function of O–O versus distance b) height of first peak of each electrolyte at 1373 K.

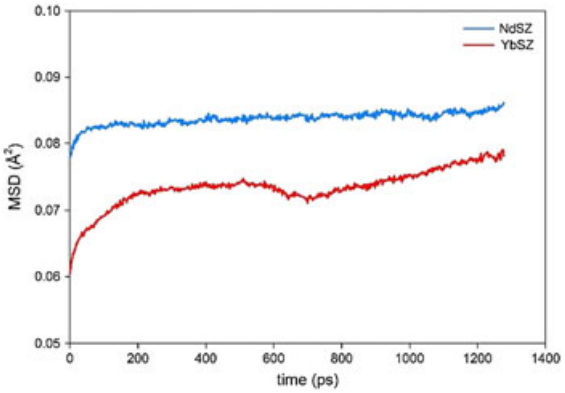

Figure 13. MSD of Zr^{4+} at 1373 K.

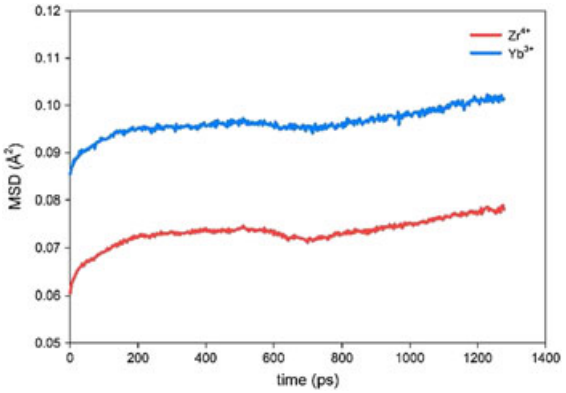

Figure 14. MSD of cations for YbSZ at 1373 K.

It was discussed that high vibration behavior of particles decreases the ionic conductivity especially at the low temperature region as can be seen in Figure 2. Vibration of cations, to some extent, may fill the vacancy and contract the free space for oxygen hopping. Therefore, there is an attempt to know the vibration of which cation is greater in an HPC plate (dopant^{3+} or Zr^{4+}). Knowing this parameter helps to find the cation in HPC that limits oxygen-hopping process. Accordingly, MSD of HPC cations was plotted for YbSZ in Figure 14 as a typical sample. It is observed that MSD of Yb^{3+} (dopant) is higher than Zr^{4+}. Consequently, movement of dopant is higher than Zr^{4+} and vacancies may be affected by dopant vibration. In other words, higher movement (or vibration) of dopant may restrict oxygen ion hopping.

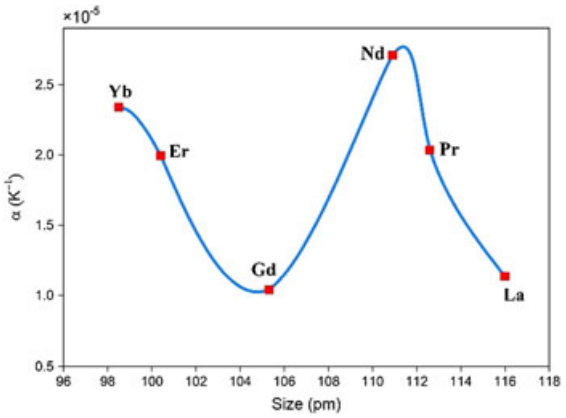

Figure 15. Thermal expansion for studied electrolytes.

3.3. Thermodynamic properties

3.3.1. Thermal expansion

One of the most important factors that must be considered for a solid oxide electrolyte is thermal expansion obtained from the slope of ln$V$ versus T. The results of thermal expansion are represented in Figure 15 for target electrolytes. These results display a quite erratic trend with size of dopant and are difficult to rationalize. As Wei *et al.* [45] mentioned, change of volume is affected by van der Waals interaction. Accordingly, thermal expansion may depend on van der Waals interaction, too. Thus, van der Waals energy would help to know what happens if dopant changes in the electrolytes. However, thermal expansion is a property which is calculated in a range of temperature not at a constant temperature. For that reason, thermal expansion is plotted versus the van der Waals energy changes (ΔE_{vdw}) as

Figure 16 shows in detail. Actually, ΔE_{vdw} was calculated over the range of studied temperature. As it is observed, thermal expansion has a linear relation with ΔE_{vdw}.

3.3.2. Specific heat capacity

Because of operating at high temperature, heat transfer is important in SOFC. Therefore, the information about heat capacity is vital to analyze heat transfer. Heat capacity is an applicable and useful parameter to calculate thermal diffusivity coefficient and has influence on startup time of fuel cell operation. In addition, zirconia-based solid oxide electrolyte with cubic structure exploits the utilization as a nuclear fuel [19]. Some thermal properties such as low thermal conductivity and high heat capacity must be considered for these purposes. Consequently, investigating heat capacity seems sound. The results of calculated heat capacity of all electrolytes as function of dopant size at the studied temperature range are reported in Figure 17. The results also explain quite erratic trend. We know that specific heat capacity is defined as the amount of heat treated to material to increase its temperature by a unit temperature (per mole). If we consider two materials with high

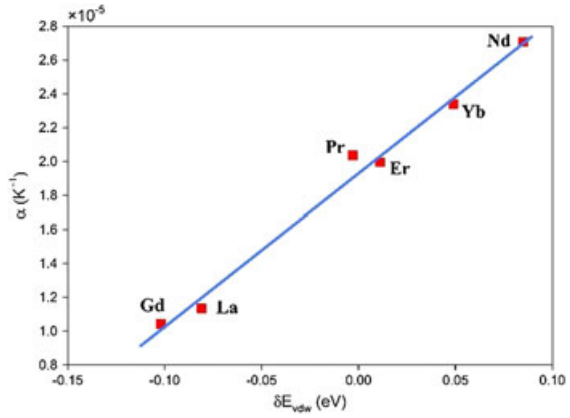

Figure 16. Thermal expansion as a function of van der Waals energy changes.

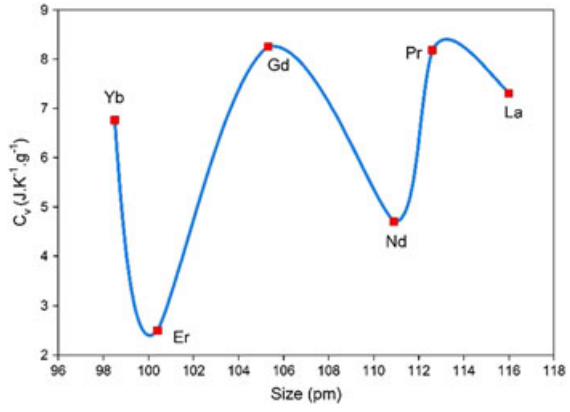

Figure 17. Heat capacity for studied electrolytes.

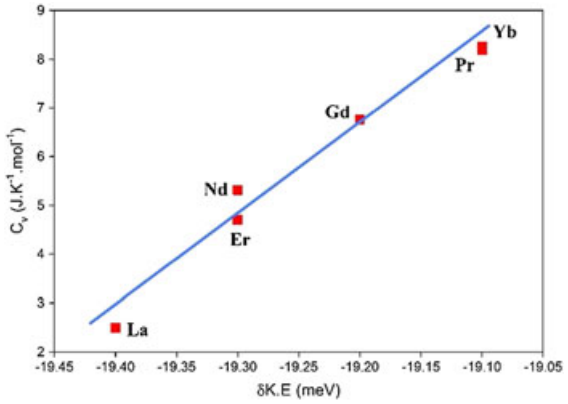

Figure 18. Heat capacity as a function of kinetic energy changes.

and low heat capacity values, then at constant heat rate the highest specific heat capacity one electrolyte has, the lowest temperature changes it should witness. We also know kinetic energy of the particle depends on temperature; consequently, it may be reasonable that specific heat capacity correlates with kinetic energy change ($\delta K.E$). The result of heat capacity as a function of $\delta K.E$ is depicted in Figure 18. As can obviously be seen, the specific heat capacity has linear correlation with kinetic energy.

4. CONCLUSIONS

Rare-earth zirconia-based electrolytes were investigated by molecular dynamics simulation in a spanning temperature of 1373 K to 1873 K in order to evaluate dynamic, structural, and thermal properties of electrolytes. Arrhenius plot of each electrolyte implies a dissimilar trend from low temperature to high one because of their different slopes. Consequently, a new aspect of applying vibrational spectra was performed to clear the darkness behind the observed slope of Arrhenius plots. Vibrational spectra of an atomic trajectory of cations and anions were examined by Fourier transform analysis of trajectory. Electrolyte with lower value of MMB points to lower vibration in HPCs, which was verified by Zr^{4+} MSD. From MSD, although the atomic mass of dopant is higher than Zr, its movement (vibration) in HPC is higher than Zr ion. Therefore, dopant vibration is responsible for MMB. There was also conducted a simple well-defined model to calculate activation energy of hopping oxygen ion to the first nearest neighbor vacancy. A system with lower vibrating HPC implies lower activation energy of oxygen. First peak of O–O radial distribution function and 001 density distribution of oxygen ions claimed activation energy of oxygen hopping has direct correlation with oxygen scattering in the lattice structure. The higher activation energy one electrolyte has the higher vibrating HPC and oxygen scattering it experiences. Thermal expansion and heat capacity were studied as important factors in heating operation. As a brilliant result, it was clear that thermal expansion and heat capacity have a direct linear relation with van der Waals and kinetic energy, respectively.

Int. J. Energy Res. 2016; **40**:1712–1723 © 2016 John Wiley & Sons, Ltd.
DOI: 10.1002/er

NOMENCLATURE

E_a	= Activation energy
r	= Atomic position
ρ_{001}	= Atomic density
k	= Boltzmann constant
φ	= Born–Mayer–Buckingham potential
V	= Cell volume
n	= Concentration of mobile ions
D	= Diffusion coefficient
r_{ij}	= Distance between atoms i and j
B	= Einstein's equation constant
$E_{relaxation}$	= Energy at relaxation point
ω	= Frequency
R	= Gas constant
H_R	= Haven ratio
C_v	= Heat capacity
q	= Ionic charge
σ	= Ionic conductivity
E_{plate1}	= Minimum energy calculated from scenario 1
$N_j(r)$	= Number of j atoms in a spherical shell
A_{ij}	= Potential parameter
C_{ij}	= Potential parameter
ρ_{ij}	= Potential parameter
σ_0	= Pre-exponential of Arrhenius equation
p	= Pressure
$g_{i,j}(r)$	= Radial distribution function (RDF)
T	= Temperature
a	= The charge of each cation
b	= The central oxygen charge
c	= The amount of negative charge of adjacent oxygen
α	= Thermal expansion coefficient
t	= Time
N_j	= Total number of j atoms
N	= Total number of all atoms
E	= Total energy
$R(\omega)$	= Vibrational spectra

List of Abbreviations

NVT	= Canonical ensemble
DOI	= Dynamic oxygen ion
ErSZ	= Erbium stabilized zirconia
GdSZ	= Gadolinium stabilized zirconia
HPC	= Hopping plate cations
NPT	= Isobaric–isothermal ensemble
$\delta K.E$	= Kinetic energy changes
LaSZ	= Lanthanum stabilized zirconia
MSD	= Mean square displacement
MMB	= Migration movement barrier
MD	= Molecular dynamics
NdSZ	= Neodymium stabilized zirconia
NHPC	= Non hopping plate cations
PrSZ	= Praseodymium stabilized zirconia
RDF	= Radial distribution function
SOFC	= Solid oxide fuel cell
SOI	= Static oxygen ion
ΔE_{vdw}	= Van der Waals energy change
YbSZ	= Ytterbium stabilized zirconia

ACKNOWLEDGEMENTS

The financial support provided by Ferdowsi University of Mashhad (grant no. 2/30461) is greatly appreciated.

REFERENCES

1. Andersson M, Yuan J, Sundén B. Review on modeling development for multiscale chemical reactions coupled transport phenomena in solid oxide fuel cells. *Applied Energy* 2010; **87**:1461–1476.
2. Lee S, Hong C. Multi-scale design simulation of a novel intermediate-temperature micro solid oxide fuel cell stack system. *International Journal of Hydrogen Energy* 2010; **35**:1330–1338.
3. Jacobson AJ. Materials for solid oxide fuel cells. *Chemistry of Materials* 2009; **22**:660–674.
4. Huang HC, Su PC, Kwak SK, Pornprasertsuk R, Yoon YJ. Molecular dynamics simulation of oxygen ion diffusion in yttria stabilized zirconia single crystals and bicrystals. *Fuel Cells* 2014; **14**:574–580.
5. Badwal SPS. Zirconia-based solid electrolytes: microstructure, stability and ionic conductivity. *Solid State Ionics* 1992; **52**:23–32.
6. Lau KC, Dunlap BI. The roles of classical molecular dynamics simulation in solid oxide fuel cells. In *InTech*, Vol. **1**. 2012; Chapter 17, p. 341.
7. Kilner J, Brook R. A study of oxygen ion conductivity in doped non-stoichiometric oxides. *Solid State Ionics* 1982; **6**:237–252.
8. Gerhardt-Anderson R, Nowick A. Ionic conductivity of CeO_2 with trivalent dopants of different ionic radii. *Solid State Ionics* 1981; **5**:547–550.
9. Arachi Y, Sakai H, Yamamoto O, Takeda Y, Imanishai N. Electrical conductivity of the ZrO_2–Ln_2O_3 (Ln = lanthanides) system. *Solid State Ionics* 1999; **121**:133–139.
10. Okazaki H, Suzuki H, Ihata K. A possibility of the oxygen diffusion enhancement in YSZ: a molecular dynamics study. *Physics Letters A* 1994; **188**:291–295.
11. Brinkman HW, Briels WJ, Verweij H. Molecular dynamics simulations of yttria-stabilized zirconia. *Chemical Physics Letters* 1995; **247**:386–390.
12. Suzuki K, Endou A, Miura R, Oumi Y, Takaba H, Kubo M, Schatterjee A, Fahmi A, Miyamoto A.

Molecular dynamics simulations on oxygen ion diffusion in strained YSZ/CeO_2 superlattice. *Applied Surface Science* 1998; **130–132**:545–548.
13. Suzuki K, Kubo M, Oumi Y, Miura R, Takaba H, Fahmi A, Chatterjee A, Teraishi K, Miyamoto A. Molecular dynamics simulation of enhanced oxygen ion diffusion in strained yttria-stabilized zirconia. *Applied Physics Letters* 1998; **73**:1502–1504.
14. Yamamura Y, Ihara C, Kawasaki S, Sakai H, Suzuki K, Takami S, Kubo M, Miyamoto A. Materials design of perovskite-based oxygen ion conductor by molecular dynamics method. *Solid State Ionics* 2003; **160**:93–101.
15. Yamamoto O, Arati Y, Takeda Y, Imanishi N, Mizutani Y, Kawai M, Nakamura Y. Electrical conductivity of stabilized zirconia with ytterbia and scandia. *Solid State Ionics* 1995; **79**:137–142.
16. Yamamura Y, Kawasaki S, Sakai H. Molecular dynamics analysis of ionic conduction mechanism in yttria-stabilized zirconia. *Solid State Ionics* 1999; **126**:181–189.
17. Hayashi H, Sagawa R, Inaba H, Kawamura K. Molecular dynamics calculations on ceria-based solid electrolytes with different radius dopants. *Solid State Ionics* 2000; **131**:281–290.
18. Schelling PK, Phillpot SR, Wolf D. Mechanism of the cubic-to-tetragonal phase transition in zirconia and yttria-stabilized zirconia by molecular-dynamics simulation. *Journal of the American Ceramic Society* 2001; **84**:1609–1619.
19. Arima T, Fukuyo K, Idemitsu K, Inagaki Y. Molecular dynamics simulation of yttria-stabilized zirconia between 300 and 2000 K. *Journal of Molecular Liquids* 2004; **113**:67–73.
20. Devanathan R, Weber WJ, Singhal SC, Gale JD. Computer simulation of defects and oxygen transport in yttria-stabilized zirconia. *Solid State Ionics* 2006; **177**:1251–1258.
21. Pramananda Perumal T, Sridhar V, Murthy KPN, Easwarakumar KS, Ramasamy S. Molecular dynamics simulations of oxygen ion diffusion and superionic conduction in ytterbia-stabilized zirconia. *Computational Materials Science* 2007; **38**:865–872.
22. Xie X, Kumar R, Sun J, Henson L. Structure and conductivity of yttria-stabilized zirconia co-doped with Gd_2O_3: A combined experimental and molecular dynamics study. *Journal of Power Sources* 2010; **195**:5660–5665.
23. Razmkhah M, Hamed Mosavian M, Moosavi F. $Nd_{2-x}Gd_xZr_2O_7$ electrolytes: thermal expansion and effect of temperature and dopant concentration on ionic conductivity of oxygen. *International Journal of Hydrogen Energy* 2014; **39**:8437–8448.
24. Razmkhah M, Hamed Mosavian MT, Moosavi F. Molecular dynamics study of complex dopant electrolyte $Nd_{2-x}Ho_xZr_2O_7$: structure, conductivity, and thermal expansion. *Fuel Cells* 2013; **13**:1048–1055.
25. Kudoh Y, Takeda H, Arashi H. In situ determination of crystal structure for high pressure phase of ZrO_2 using a diamond anvil and single crystal X-ray diffraction method. *Physics and Chemistry of Minerals* 1986; **13**:233–237.
26. Mandal B, Dutta A, Deshpande S, Basu R, Tyagi A. Nanocrystalline $Nd_{2-y}Gd_yZr_2O_7$ pyrochlore: facile synthesis and electrical characterization. *Journal of Materials Research* 2009; **24**:2855–2862.
27. Mandal B, Deshpande S, Tyagi A. Ionic conductivity enhancement in $Gd_2Zr_2O_7$ pyrochlore by Nd doping. *Journal of Materials Research* 2008; **23**:911–916.
28. Thangadurai P, Sabarinathan V, Chandra Bose A, Ramasamy S. Conductivity behaviour of a cubic/tetragonal phase stabilized nanocrystalline La_2O_3–ZrO_2. *Journal of Physics and Chemistry of Solids* 2004; **65**:1905–1912.
29. Strickler D, Carlson W. Electrical conductivity in the ZrO_2-rich region of several M_2O_3–ZrO_2 systems. *Journal of the American Ceramic Society* 1965; **48**:286–289.
30. Gunn DS, Allan NL, Purton JA. Adaptive kinetic Monte Carlo simulation of solid oxide fuel cell components. *Journal of Materials Chemistry A* 2014; **2**:13407–13414.
31. Ewald PP. Die Berechnung optischer und elektrostatischer Gitterpotentiale. *Annalen der Physik* 1921; **369**:253–287.
32. Li Z-P, Mori T, Ye F, Ou D, Zou J, Drennan J. Ordered structures of defect clusters in gadolinium-doped ceria. *The Journal of Chemical Physics* 2011; **134**:224708.
33. Lewis G, Catlow CRA. Potential models for ionic oxides. *Journal of Physics C: Solid State Physics* 1985; **18**:1149–1161.
34. Berendsen HJ, Postma JPM, van Gunsteren WF, DiNola A, Haak J. Molecular dynamics with coupling to an external bath. *The Journal of Chemical Physics* 1984; **81**:3684.
35. Verlet L. Computer "experiments" on classical fluids. I. Thermodynamical properties of Lennard–Jones molecules. *Physical Review* 1967; **159**:98.
36. Smith W. Guest Editorial: DL_POLY-applications to molecular simulation II. *Molecular Simulation* 2006; **32**:933–933.
37. Smith W, Forester TR. DL_POLY_2.0: a general-purpose parallel molecular dynamics simulation package. *Journal of Molecular Graphics* 1996; **14**:136–141.
38. Tung KL, Chang KS, Hsiung CC, Chiang YC, Li YL. Molecular dynamics simulation of the complex dopant effect on the super-ionic conduction and microstructure

of zirconia-based solid electrolytes. *Separation and Purification Technology* 2010; **73**:13–19.
39. Murch GE. The haven ratio in fast ionic conductors. *Solid State Ionics* 1982; **7**:177–198.
40. Kreyszig E. *Advanced Engineering Mathematics*, tenth Edition. John Wiley & Sons, 2010; Chapter 11, p. 523.
41. Atkins PW, De Paula J. *Physical Chemistry*, Vol. **8**. Oxford University Press: Oxford, 2006; 62.
42. McQuarrie D. *Statistical Mechanics*. Harper and Row: New York, 1976.
43. Shannon R. Revised effective ionic radii and systematic studies of interatomic distances in halides and chalcogenides. *Acta Crystallographica Section A: Crystal Physics, Diffraction, Theoretical and General Crystallography* 1976; **32**:751–767.
44. de Silva CW. *Vibration: Fundamentals and Practice*, Second Edition. Taylor & Francis: 2006; Chapter 4, p. 179.
45. Wei C, Srivastava D, Cho K. Thermal expansion and diffusion coefficients of carbon nanotube-polymer composites. *Nano Letters* 2002; **2**:647–650.